We are IntechOpen, the world's leading publisher of Open Access books Built by scientists, for scientists

4,800
Open access books available

122,000
International authors and editors

135M
Downloads

Our authors are among the

154
Countries delivered to

TOP 1%
most cited scientists

12.2%
Contributors from top 500 universities

CLARIVATE ANALYTICS BOOK CITATION INDEX INDEXED

WEB OF SCIENCE™

Selection of our books indexed in the Book Citation Index in Web of Science™ Core Collection (BKCI)

Interested in publishing with us?
Contact book.department@intechopen.com

Numbers displayed above are based on latest data collected.
For more information visit www.intechopen.com

6

Functional Implication Guided by Structure-Based Study on *Catalase-Peroxidase* (KatG) from *Haloarcula Marismortui*

Takao Sato
Depertment of Life Science, Graduate School of Bioscience and Biotechnology, Tokyo Institue of Technology, Midori-ku, Yokohama Japan

1. Introduction

The *catalase–peroxidase* (KatG; EC 1.11.1.7) has a variety of roles in different organisms, which distributes widely among fungi, bacteria and archaea. However, the protein sequences of all procaryotic KatGs belong to a member of the class I *peroxidase* superfamily involving Cytochrome c *peroxidase* (CcP) and Ascorbate *peroxidase* (APX) (Welinder, 1991, 1992). As indicated by the enzyme name, KatG is a bi-functional enzyme exhibiting both *catalase* and *peroxidase* activities to prevent potential damage to cellular components by exogenous hydrogen peroxide (H_2O_2) and its deprotonation product. KatG is also interested in its involvement of the activation of anti-*tuberculotic* pro-drug isonicotinic acid hydrazide (isoniazide, INH) (Bertrand et al., 2004). INH is activated as its *peroxidase* substrate by KatG from *Mycobacterium tuberculosis* (*Mt*). Resulting radical via oxidation (Zhang et al., 1992; Heym et al., 1993) prevents growth of the pathogenic microorganism by inhibiting the synthesis of mycolic acid component of the mycobacterial cell wall. *Mt*KatG shares 55% identity and 69% similarity in its amino acid sequence with KatG from *Haroarcula marismortui* (*Hm)* as homologous protein. Reaction process of *catalase* and *peroxidase* activities in the heme-containing hydroperoxidases including class I, class II (fungus lignin *peroxidase*), class III (classical secretory *peroxidase*, example being horseradish *peroxidase*) enzymes and manmalian liver *catalase* is explained uniformly (Hillar et al., 2000). Ionic (heterolytic) cleavage of the first H_2O_2 molecule on the heme iron leads to compound I formation, an oxyferryl-radical cation intermediate [Fe^{IV}=O–Por(•+) or Fe^{IV}=O–Por–aa(•+), aa: side-chain of amino acid of Tyr218(Y218) or Trp95(W95) (all numbering is for *Hm*KatG unless otherwise stated)], is the first step of hydroperoxidase reaction as reaction 1. KatG forms a Por(•+) as well as Y218 and W95 radicals in the absence of reducing substrate (reaction 2; Ivancich et al., 2003). In *peroxidases*, compound I is reduced in two sequential one-electron transfers, usually from donor (AH, *O*DA: *o*-dianisidine), and involve an intermediate called compound II (reactions 3 and 5). Two resonance structures for compound II could exist (reaction 4).

$$\text{KatG}\,[\text{Por}-\text{Fe}^{\text{III}}] + \text{H}_2\text{O}_2 \rightarrow \text{Compound I}\,[\text{Por}\bullet-\text{Fe}^{\text{IV}}=\text{O}] + \text{H}_2\text{O} \qquad (1)$$

$$\text{Compound I}\left[\text{Por}\left(\bullet^{+}\right)-\text{Fe}^{\text{IV}}=\text{O}\right]\leftrightarrow\text{Compound I}\left[\text{Por Y218}\left(\bullet^{+}\right)-\text{Fe}^{\text{IV}}=\text{O}\right]\leftrightarrow \\ \leftrightarrow\ \text{Compound I}\left[\text{Por W95}\left(\bullet^{+}\right)-\text{Fe}^{\text{IV}}=\text{O}\right] \tag{2}$$

$$\text{Compound I}\left[\text{Por}\left(\bullet^{+}\right)/\ \text{Y218}\left(\bullet^{+}\right)/\ \text{W95}\left(\bullet^{+}\right)-\text{Fe}^{\text{IV}}=\text{O}\right]+\text{AH}\rightarrow \\ \rightarrow\text{Compound II}\left[\text{Por}-\text{Fe}^{\text{IV}}=\text{O}\right] \tag{3}$$

$$\text{Compound II}\left[\text{Por}-\text{Fe}^{\text{IV}}=\text{O}\right)]\leftrightarrow\ \text{Compound II}\left[\text{Por}-\text{Fe}^{\text{III}}-\text{OH}\right] \tag{4}$$

$$\text{Compound II}\left[\text{Por}-\text{Fe}^{\text{IV}}=\text{O}\right]+\text{AH}\rightarrow\text{KatG}\left[\text{Por}-\text{Fe}^{\text{III}}\right]+\text{H}_2\text{O}+\text{A} \tag{5}$$

$$\text{AH}\left[\text{ODA}\ /\text{ODA}\ (\bullet^{+})\right]\rightarrow\text{A}\left[\text{ODA}_{\text{red}}\right] \tag{6}$$

One of the most common causes of INH resistance is the Ser305Thr (S305T) mutation and, while remaining significant *catalase* and *peroxidase* activities, the [S305T] variant enzyme maintains the equivalent affinity for INH (Musser et al., 1996; Haas et al., 1997; Dobner et al., 1997; Marttila et al., 1998; Wengenack et al., 1997; Heym et al., 1995). The *Mt*KatG [S305N] variant completely lost the ability to convert INH into the InhA inhibitor (Wei et al., 2003). A role for the radicals in activation of the antibiotic is known to proceed by one-electron oxidation producing drug-based radical intermediates (Slayden & Barry III et al., 2000). It indicates that the direct reduction of compound I KatG by INH with pyridine ring is arguing against an activation mechanism requiring amino-acid based radicals. Structural and functional information is available for the crystallographic, kinetics and site-directed mutagenesis studies for *Hm*KatG. The crystal structure of wild-type (WT) *Hm*KatG, [S305T] or [S305A], [R409L], and [M244A] variants is reported otherwise (Sato et al., to be submitted; 2011a; 2011b; 2011c; 2011d). Both *catalase* and *peroxidase* activities of *Hm*KatG [S305T] have the equal to or lower than those of WT (Sato et al., 2011a; 2011b. [S305A] variants exhibit the equal to or lower *catalase* and the equal to or higher *peroxidase* activities, respectively, than those of WT (Sato et al., 2011c). [S305A] would yield the prospective complexes with aromatic inhibitor for the higher affinity than that of [S305T]. [R409L] variant, in Arg substitutions of Arg409 to Leu, reveals the higher *peroxidase* property. These structures in combination with the biochemical characterization of variants lead to identify a few of KatG-specific residues, including the cross-linkage covalent adduct among W95, Y218 and M244, unique to KatGs, G99, Y101, D125, and E194, which is conserved across all KatGs. The mechanistic aspects of KatG catalysis and kinetic studies on site-directed mutagenesis from *Hm* of equivalent variants from *Mt* have allowed a fully quantitative rationalization of the *catalase* reactivity of [S305T] and [R409L] for *Hm*KatG (Sato at al., 2011a). The structure-based computational techniques have provided a mechanistic framework that the binding affinity and rate of turnover for H_2O_2 of these enzymes may be controlled by bonding (or nonbonding) frontier-orbital due to the presence (or absence) of π-orbital overlap between W95 and Heme. Based on the structures of *Hm*KatG [R409L] variant complexes with (electrophilic reagent) substrate for *o*-dianisidine (*O*DA) and (nucleophilic) inhibitor for cyanide anion (CN^-), the elevated *peroxidase* reactivity is gained in binding *O*DA from reorientation of the side-chain of specific residues in D125, W95 and heme (Sato et al., 2011b). The inhibition of both H_2O_2 and *O*DA is observed by such as CN^-

and salicylhydroxamic acid (2-hydroxybenzohydroxamic acid; SHA) with phenolic ring that are classical heme enzyme inhibitor, respectively, and an inhibitor of compound II KatG with respect to substrate aromatic donor as *O*DA with dimeric phenolic rings, leading to insight to INH with pyridine ring. SHA and exogenous heme iron ligands compete in binding to the resting enzyme, while phenolic substrates (phenol, p-cresol, and resorcinol) do not competitively inhibit liganding to the heme iron (Modi et al., 1989; Ikeda-Saito et al., 1991). The aromatic substrate binding site on heme iron has been identified by determining the structures of [S305A] and its complexes with SHA. These provide a complete description of substrate binding in KatG (Sato et al., 2011b; 2011c). It is implied for SHA inhibition reaction that the proposal model of INH- *Mt*KatG complex may share structural similarity with SHA in binding site of *Hm*KatG [S305A] variant. Hence, *Hm*KatG [S305T] or [S305A] and [R409L] variants are expressed with an attempt at rational catalytic redesign, to prepare the inhibitor- or substrate-enzyme complex, because the [S305A] and [R409L] variants are expected to have the higher affinity for SHA and *O*DA than that of the WT, respectively, and exhibits the equal to or higher *peroxidase* activity than that of WT.

On the other hand, in [R409A], [R409K], and [R409L] variants of other KatGs, the *catalase* activity decreased while the *peroxidase* activity did not affected (Carpena et al., 2005; Jakopitsch et al., 2004; Ghiladi et al., 2004). One of the commonest causes of resistance about INH is also the [R409L] mutation in *Mt*KatG and known for *peroxidase* reaction (Ghiladi et al., 2004; Saint-joanis et al., 1999). It is required for [R409L] equivalent variants from *Hm*KatG to be increasing sensitivity to *O*DA and, activating significant *peroxidase* while remaining slightly *catalase* activities (Sato et al., 2011a; 2011b). The single-base mutation between [R (cgg) 409L (ctg)] and [S (agc) 305T (acc)] would be possible from mutational events in natural evolution. It is expected that attempts to generate a "new" function within a laboratory time scale can imitate the entire process used by Nature to evolve and optimize a new function, but these studies illustrate that the acquisition of sequential mutations can produce a continuous pathway for evolution of a "new" function (*peroxidase* here).

Notably, KatG-specific Met244 sulfur coordination to two carbonyl backbone of Tyr101 (Y101) and Gly99 (G99) and including Tyr218, Trp95 on the distal side of the heme, the unique covalent modification among the side chains of three amino acids (M244, Y218 and W95) are present. It was reported that additionally, phenyl oxygen (Oη) of Y218 and amide nitrogen (N) backbone of M244 in the covalent adduct have hydrogen (H)-bonds with the guanisyl N*ε1* and Nε2 of Arg409 (R409), respectively (Yamada et al., 2002). The covalent adduct has been shown to be generated by autocatalytic process (Ghiladi et al., 2005a). Crystallographic analysis of KatG from *Bulkhorderia pseudomallei* (*Bp*) has indicated that the side-chain of R409 (corresponding to *Hm*KatG numbering) shows conformational change depending on both of pH and the physicochemical state of the active site (Carpena et al., 2005). Five amino acid residues, Y101, G99, M244, Y218, and W95 are conserved in all the KatGs but not in the other class I *peroxidases*. [W95A], [W95F], and [M244I] variants in KatG from *Synechocystis* (*Sy*) or [M244A], [M244L] in *Bp*KatG considerably decreased the *catalase* activity, whereas the *peroxidase* activity was even enhanced (Regelsberger et al., 2000; Jakopitsch et al., 2004; Singh et al., 2004). It has a slight difference in [M244A], [M244L] variants in *Bp*KatG and [M244I] variant in *Sy*KatG. Substitution of Tyr218 to Ala [Y218A] or Phe [Y218F] in the M244–Y218–W95 covalent adducts induced complete loss of the *catalase* activity, whereas the *peroxidase* activity was highly enhanced in *Sy* KatG (Jakopitsch et al., 2003a; Jakopitsch,et al., 2003b). M244 in the adduct also has any significant role in the enzyme, whereas the substitution of

Met to Ile considerably attenuated the *catalase* activity but did not lose at all, and enhanced the *peroxidase* activity (Jakopitsch et al., 2004; Singh et al., 2004). Site-specific mutagenesis indicated that the covalent adduct and its relevant was significant to the *catalase* activity, whereas their effect on the activity was complicated and was hardly explained. Substitution for [M244A] affected the *Hm*KatG structure of the access channel and therefore the enzymatic parameters for the *peroxidase* activity (Ten-i et al., 2007). This mutation also induced the significant functional change in the active site that would trigger a loss of *catalase* activity and a high enhancement of *peroxidase* activity (Sato et al., 2011d). It was also investigated whether the absence of the structural feature unique to KatG, namely M244–Y218–W95 adduct in which are covalently linked together through these side chains, can be correlated with exhibiting the *peroxidase* reactivity. Resulting in the [M(atg)244A(gca)] substitution, the designed three-base mutation leads to cleavage the covalent bond between M244 and Y218–W95, as was identified in the adducts. It has been constructed the successive triple-base substitution of Met244 to Ala [M244A] and to cleavage the covalent bond amongst M244–Y218–W95 adduct, though this variant would not be expected in natural evolution. Using rounds of site-specific mutagenesis coupled with the structure based-evolution, the unique access will be provided to structural changes that allow enhancement and eventual optimization of the "new" function.

In this paper, the structure-based computational chemical technique can confirm a fully quantitative rationalization of the reactivity mechanism of electron transfer (ET). Interestingly, it was strongly suggested by this structure-base calculation that this variant did not alter compound I formation but can have capacity to restore compound I from compound II, possibly suggesting a yet-to-be defined mechanism for *peroxidase* that can be allowed to perform in *Hm*KatG.

2. Materials and method

2.1 Structure based molecular orbital and docking analyses

Starting structure models contained 370 atoms for WT *Hm*KatG, 375 atoms for [S305T], 385 to 389 atoms between [S305A] and SHA–[S305A], 368 to 405 atoms among [R409L], CN–[R409L], CN – [R409L] complexes with *O*DA and 364 atoms for [M244A], after hydrogen addition to their crystal structures. The residues were confined to the immediate vicinity (surrounded around 3.6Å) among the heme and ligand coordinate of G99 or Y101, M244-Y218-W95 covalent linkages adduct. Geometries were determined by mechanics optimization using augmented MM3. The semi-empirical molecular orbital (MO) method was performed by a MOPAC2002 program / AM1 wavefunction (Stewart, 2002; Dewar et al., 1985). All the sets of molecular orbitals are generated from the highest occupied molecular orbital (HOMO) to the lowest unoccupied molecular orbital (LUMO), exhibiting the negative value for MOPAC-specific calculation. When ionization energy (HOMO) is greater than -8 eV including with HOMO density, electrophilic frontier orbital density (fr) and electrophilic superdelocalizability (Sr), the residues have the electrophilic reactivity. Electron affinity (the LUMO) for nucleophilic group is less than that of -2eV with LUMO density, nuclophilic fr and nuclophilic Sr, exhibiting the reactive indices, fr and Sr to be most reactive (Fukui et al., 1954; 1957) with the excitation of electron in the energy gap. An π–electron is transferred from HOMO to LUMO, when HOMO and LUMO polarities are homologous and uniformed, the geometries of the HOMO/LOMO states that have the distance within 3.4Å of van der Waals contact, the matching phases (overlapping the

bonding orbitals) and the gap energies within 6eV (Pearson, 1986). It is assumed that the π-electron delocalization of adduct might influence ability of the intrinsic properties of KatG to transfer electron in its conjugate system and then to exhibit the *catalase* activity (Sato et al., 2011a). For understanding the chemical reactivity and site, the MO calculations were carried out on a PC using BioMedCAChe ver6.1.12.34 (Fujitsu, Tokyo). The outcomes of the *in vacuo* calculations on coordinate complex, covalent adduct and heme are related to the electronic characteristics of the covalent adducts, SHA, and *O*DA which bound to heme into the hydrophobic cleft of the variants and its complexes. *O*DA as a *peroxidatic* substrate and an electron in the HOMO of the donor molecule as *O*DA ($\cdot^{+}$) cation radical is transferred to the LUMO in the heme of compound I. The reverse is also taking place for SHA.

In addition, when it was difficult for the value of K_m (substrate affinity) to measure, conveniently it was quantified by binding energy calculated from the docking study. The binding energy for a given ligand (ΔE_{ligand}) can be expressed in (eq.7) as the difference in the energy between complex and components (Fukuzawa et al., 2003).

$$\Delta E_{ligand} = E_{complex} - \left(E_{enzyme} + E_{ligand}\right), \tag{7}$$

where are the heat of formation energy of each of the three systems, i.e., E_{ligand} of H_2O_2, SHA, or *O*DA and, E_{enzyme}, of the KatG enzyme, and $E_{complex}$ of the enzyme complexes with H_2O_2, SHA, or *O*DA. The binding energy can be estimated to subtract the sum of heat of formation energy values of each system from that of pair of an enzyme and a ligand.

It is indicated that H_2O_2 molecule leads to compound I formation on the heme iron. In docking exogenous ligands to heme, the binding energy between ligand (H_2O_2 as an initiator, SHA as an inhibitor of *peroxidase* compound I and *O*DA as *peroxidase* substrate) and enzyme can be approximately estimated from the relative energy difference which subtracts each heat of formation calculated between H_2O_2, SHA, *O*DA and enzyme from that of ligand–enzyme complex.

3. Results and discussion

3.1 Coordinate, covalent-adduct, heme distal side in the active center and substrate access channel

The heme moiety of the [R409L] variant is found to be deeply buried inside the *Hm*KatG and *O*DA as the *peroxidase* substrate can access to the active centre only through the narrow cylindrical channel with ~20Å depth from the entrance to the bottom, as shown in Fig1. Side-chain of Asp125 located at the bottom of the channel and showed the structural change in [R409L] complexes with *O*DA.

As shown in Fig. 2(a), the access channel was composed of LL1 loop, *helices B* and *E*, which involved in the active site of R92, H96, and heme. There is three KatG-specific structural characteristics, which consist of first component (π–complex between W95 and Heme), second component (M244–Y218–W95 covalent adduct) and third component (sulfur cation radical centered coordinate complex). One of the unique structural features (of G99, Y101, M244–Y218–W95 covalent adduct and N126) have been revealed in the structures of WT *Hm*KatG, [S305T], [S305A] and [R409L]. It consists of the octahedral (six) coordinate sulfur radical cations (>S$^{\bullet+}$) center of M244 which is capped at the *N-ter* end of *Helix E* by a

positively charged amino acid in order to neutralize this helix dipole, ligands among phenyl carbon of (KatG specific) Y218 –W95, carbonyl oxygens of Y101 (KatG specific) and G99 **(**KatG-typical and conserved with APX) at the *C-ter* end of the *Helix B* in KatG. SHA—[S305A] complex shows the phenolic group oxygen of SHA to be of 3.2Å within van der Waals contact with the the δ-heme edge. In *O*DA— [R409L] complex, the *δ*-heme edge is also confirmed as the primary site oxidation of *O*DA. The phenol ring part of SHA in the [S305A] overlaps and binds to the equivalent binding site as one aniline ring part of *O*DA in the [R409L] variant (Fig.2(b)).

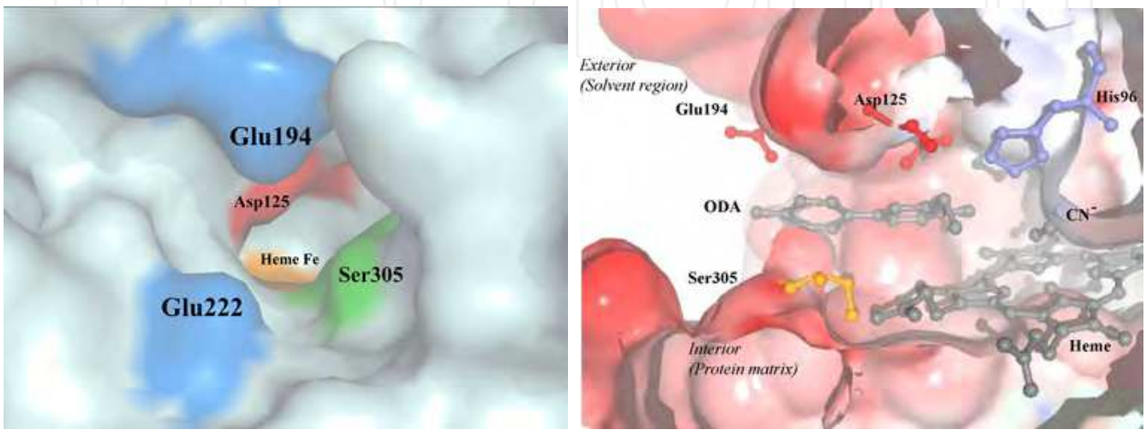

(a) (b)

Fig. 1. Active and *O*DA Binding Sites of *Hm*KatG. (a; left panel) Space-filling representation of the binding site in showing locations of the five critical residues, Glu194 and Glu222 (blue), Ser305 (green), Asp125 (red) and heme iron (orange). (b; right panel) The vertical cross-sectional view of active site of *O*DA and CN (gray), surrounded with the residues His96 (cyan), Asp125 and Glu194 (red), Ser305 (yellow) and heme (gray). These figures were constructed using MolFeat v3.0 (FiatLux Corp., Tokyo, Japan).

As shown in Fig.3 (A), entering the distal side cavity of [M244A] variant through the constricted portion of the channel, the initiator H_2O_2 would come into contact with the active-site residues W95 and H96 on *Helix B* (§3.6 *vide infra* in Table 5). While the WT, [S305T], [S305A], and [R409L] variants have been stabilized LL1 loop by covalent adduct linkage between Y218 on the mobile LL1 and M244 on *Helix E*, the [M244A] exhibits the cleavage of the linkage with Y218. When the displacement of E194 and E222 was not endured by the flexible response of the mobile D125 of upstream residues to the downstream portion of LL1 loop, it allows the mouth of the channel to open and to facilitate adequate uptake of substrate into the heme cavity. Side-chains of E194 and E222 on LL1 loop locates at the entrance of the channel and was also affected by this mutation. In subunit A, the side chain D125 disrupted H-bonding interaction with amino nitrogen of backbone I217 in the LL1 loop and the side oxygen O*δ1* formed H-bond with its own carbonyl oxygen in backbone of D125, resulted perpendicular rotation of χ2 of side D125 to face the imidazole of H96 (Fig. 3 (B)) while D125 has been known to be important in the H_2O_2 oxidation to date (Jakopitsch et al., 2003a; Singh et al., 2004). However, there is a displacement of 2.69Å toward 2.80 Å and dramatic reversal of the dihedral angle χ2 of side D125, which is to bind *peroxidase* substrate as *O*DA or water molecule as deriving

from H_2O_2, respectively. Hence, the mobile D125 residue will also be suggestive of utilizing as either initiator H_2O_2 or substrate *O*DA recognition, making it effective in binding substrate, though disruption of π-complexes with heme and W95 known to act on as molecular switch from the *catalase* to the

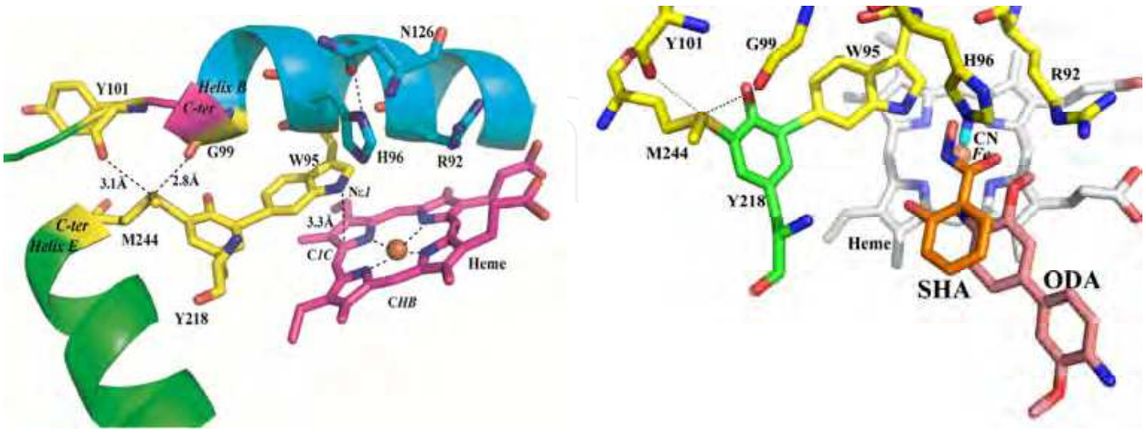

(a) (b)

Fig. 2. (A) Helixes B and E, the 6th Coordinate, the Covalent Adduct and Heme π-complexes in Active Site Structure of WT, and three variants. (B) Structure-based Overlays of the [S305A]–SHA and Cyanide [R409L]–*O*DA complexes. (a; left panel).The distal R92, H96, N126 on Helix B are shown in blue, W95 on Helix B, Y218 and M244 on Helix E residues in yellow. Heme is shown in purple and orenge sphere represent heme iron atom. The π—π* stacking interaction between W95 and Heme is represented by dashed line between N*ε1*, respectively, and C*1C* atoms near α-meso heme edge. The H- and coordinated-bonds for the structures of [WT], [S305T], [S305A] and [R409L] are represented by dashed lines (black). (b; right panel).The ligand structures are coincided with δ-meso heme edge and are avoided overlap considerably between the inhibitor SHA (yellow) and substrate *O*DA (magenta). The heme is shown in gray, and two residues, W95, H96 and R92, which involved in the binding site for the [S305A] and [R409L], directly superimposed in all cases; for clarity, only one residue is indicated. The coordinated-bonds for the S305A-SHA structure are represented by dashed lines (black).

peroxidase (Carpena et al., 2005). The amino N of backbone I217 forms an H-bond to the oxygen O*δ1* of carbonyl group of the side D125. Thus no H-atom can be in the C=O*δ1* group. When O*δ2* of the D125 can be an ionized carboxyl group at optimum pH6 near pKa value of 4.0, it may be a powerful proton donor for binding the *peroxidase* substrate with extremely high affinity (Km^A = 0.974 μM) for *O*DA would be attributed to rotate the dihedral angle χ2 by 61.3° of the mobile side D125 in the subunit A of [M244A] variant. Hence it reorients the sp^2 orbital of the –O*δ2* (-H) which functions as powerful proton acceptor and has a high affinity for the *O*DA molecule, when the *sp* orbital of the —C=O*δ1* which acts as proton donor and a lower affinity for H_2O_2 molecule. The role of D125 may form the binding site for the water molecule which derived from the first H_2O_2 molecule (and then compound I formation), may carry its water molecule out of the active site and may induce and control entry of the second *O*DA molecule into the cavity. In other words, O*δ1* with *syn* lone pairs binds *O*DA molecule. The one (*syn*) direction of lone pairs of the carbonyl oxygen (–C=O*δ1*) of side D125 form the more stable H-bind with cation of *O*DA

rather than that of another (*anti*) direction bound with the amide nitrogen (–NH) of backbone I217 respectively. Thus, it is also indicated by *ab initio* quantum chemical studies that *syn* protonation from (–C=O*δ1*) is more favorable to (C–O*δ2* –H) than *anti* protonation, implying the *syn* lone pairs are more basic and therefore bind *O*DA more readily than do the anti lone pairs (Petersen and Csizmadia, 1979). While the side chain of D125 is rotated around the dihedral angel χ2, since the oxygen orbital changes between (–O*δ2*-H) sp^2 and (=O*δ1*) *sp* is caused with and without *O*DA respectively, the *O*DA is bound to the *δ*–meso heme edge by the molecular mechanics and orbital changes of the D125. The D125 has different affinity for *O*DA from either strong subunit A or weak B, respectively, and facilitates the uptake of *O*DA in *peroxidase*, with draining away the water molecule. Therefore, the geometry of side chain of D125 in subunit A allows for higher binding affinity for *O*DA molecule than that of subunit B, which is consistent with the *peroxidase* in the [R409L] (Sato,T., et al., 2011b).

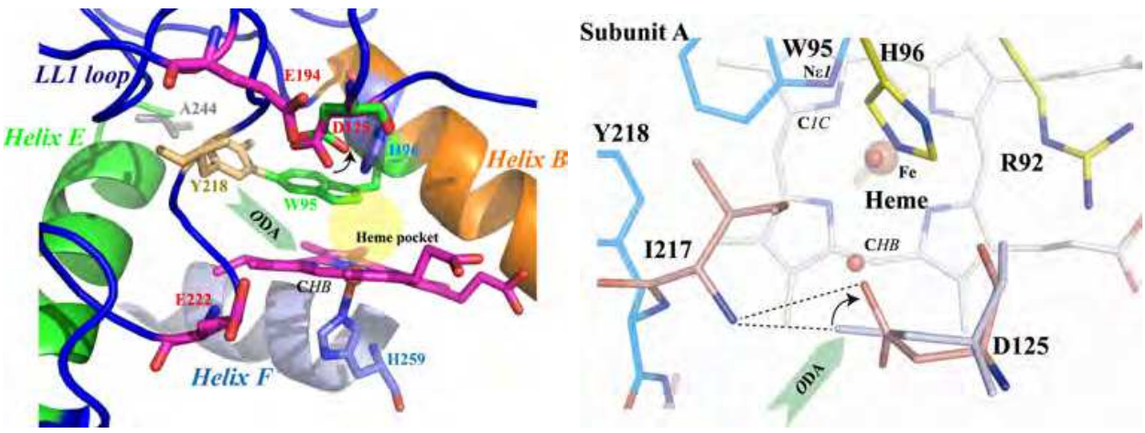

(a) (b)

Fig. 3. (A) Proposed Active Site Structure in [M244A] variant. (B)The mobile D125 in subunit A superposed that of WT. (a; left panel)In Subunit B of [M244A] variant, the distal H96 (on helix B; orange) is shown in blue. The W95 (on helix B), Y218 (on LL1 loop; cyan) and A 244 (on helix E; green) residues are in green, orange, and gray. The heme and its iron atom are represented in magenta sticks and orange sphere. The latent access channel residues of D125, E194 and E222 locate on LL1 loop, showing in red (left panel). (b; right panel) In subunit A of M244A, the Mobile D125 and I217 in pink, distal R92 and H96 are presented in yellow, the Y218 and W95 covalent adduct in cyan. The nitrogen, oxygen and heme iron atoms are colored for dark blue, red, and orange. D125 in subunit B is superimposed in colored blue, white and water molecule is shown as red spheres. The figure is view from the distal side of left panel. The figures were constructed using Pymol (DeLano, 2002).

3.2 Docking and molecular orbital calculations on ODA among WT, S305T and R409L variants

While the difference between [S305T] and [R409L] crystal structures are very subtle changes (with overall root mean square deviation of 0.492 Å) and the structural integrity is highly maintained, the binding energy of such *peroxidatic* substrate as *O*DA appears to affect functioning of the enzyme. Each of WT *Hm*KatG and [S305T] variant structures had not exhibited as a potential active site for *O*DA substrate at all. Since the propionate carbonyl

group of heme was H–bonded with either the hydroxyl group of Ser or Thr305, it assumed that it would interfere with the transport of *O*DA and cause a blockage of the channel. A calculated binding energy in the [R409L] variant (subunit A for -27.6 kcal/mol; B for -73.3 kcal/mol, which is negative and can be discussed by the magnitude of its absolute value as the following from here) also reveals to have significantly high affinity for *O*DA (Table 1) and a possible site has been proposed for [R409L] KatG, in a cavity on the distal side of the heme. Consequently, it is suggested that the porphyrin carbon atom (C*HB*) of *δ*-meso heme edge may serve as a docking site for *O*DA. Neither *catalase* nor *peroxidase* activities may be expected from docking energy (and site) in [S305T]. The promising *peroxidase* despite a lack of *catalase* activity in [R409L] may result from the localized electronic state of the heme, arising from the H–bonding interaction with *O*DA.

	WT		S305T		R409L	
Subunit	A	B	A	B	A	B
Affinity of *O*DA for *Peroxidase*						
E222–D125(kcal/mol)					-27.6	
D125–Heme (kcal/mol)						-73.3

Table 1. *O*DA binding affinity against the docking calculation. It is suggested as binding affinity that the value of ΔE_{ligand} is negative to be predicted by docking calculation with the substrate *O*DA, according to eq.7.)

Only when there are very subtle conformational changes with side-chain of residues and without backbone distortion in the substrate access channel, this structure-based molecular orbital (MO) calculation method appears to provide a useful means of assessing ET pathways and reactivity in heme-containing system. Therefore, an advantage of *semi–empirical* calculation is the ability to calculate the energies of all the MO of the individual active residues in the protein, which may be expected to be practically much better than no data obtained overtime by *ab initio* molecular orbital study combined with the large scale computer system of supercomputer.

By examining each subunits of [R409L] structure, the C*HB* atom is the most reactive site in heme that has electron–withdrawing group, where exhibits as well or greater energy of LUMO, e.g. the eigenvalues of LUMO molecular orbital has -1.43eV and -1.12 eV (Table 2) than those of WT with Subunit A of -1.79 eV and B of -1.96 eV (Table 4). Additionally, such index *peroxidase* reaction as LUMO density (0.15, 0.153), nucleophilic frontier fr (for subunit A of 0.023 and B of 0.004), and nucleophilic Sr (0.891, 0.943) in [R409L] are indicative of either equaling or surpassing the corresponding parameters (0.058, 0.159; 0.001, 0.017; 0.832, 0.912) to WT. The most likely site of binding *peroxidase* substrate would be the C*HB* atom in the δ-meso heme edge where is consistent with *O*DA recognition site suggested by the docking study in the prospective *peroxidase* activity. It may be possible to determine the geometries (phases and energies) of the states that would lead to *peroxidase* activity. It is indicated that the electronic nature of the compound I might be different as could be the mechanism of H_2O_2 oxidation. Reduction of compound I rather than compound I formation by KatG is the intersection point of the *peroxidase* and *catalase* cycle.

		WT		S305T		R409L	
Subunit		A	B	A	B	A	B
	Catalase						
	π–complex						
LUMO (eV)	W95 (N*ε1*)			-1.15	-0.26		
HOMO (eV)	Heme (C*1C*)			-6.71	-5.10		
The π-π* energy gap (eV)				5.56	4.85		
LUMO (eV)	Heme (C*1C*)	-1.05	-1.60	-2.22	-1.49	-1.43	-1.31
HOMO (eV)	W95 (Nε1)	-7.61	-7.77	-8.75	-7.74	-7.50	-7.47
The π-π* energy gap (eV)		6.56	6.17	6.53	6.25	6.07	6.16
	Octahedoral	Coordinate		complex			
LUMO (eV)	G99,Y101,Y218	-2.88	-2.84	-2.22	-2.64	-2.49	-1.93
HOMO (eV)	M244	-7.32	-7.48	-7.17	-7.28	-7.21	-7.47
HOMO-LUMO gap (eV)		4.44	4.64	4.95	4.64	4.72	5.54
	Peroxidase						
LUMO(eV)	Heme C*HB*	-1.73	-1.96	-1.62	-1.48	-1.43	-1.12

Table 2. The frontier molecular orbital of (a) HOMO and (b) LUMO Energies for Active Site Associated with *Catalase* and *Peroxidase* Reactions in WT *Hm*KatG, [S305T] and [R409L] variants.

3.3 Active sites confirmed by structure based on cyanide R409L complex with or without ODA

The *peroxidase* substrate acts as the electron donor in the *peroxidase* reaction. In the *O*DA substrate, the geometry is confined to the biphenyl and binitrogen moieties. The reaction point in *O*DA ($^{\bullet+}$) cation radical is also confined to one side of the central part of molecule. When one electron goes from neutral *O*DA to the *O*DA ($^{+}$) positive ion or when changing from the *O*DA ($^{\bullet}$) neutral radical to the *O*DA ($^{\bullet+}$) radical-cation states, the *O*DA molecule undergoes a strain reduction of bicyclic geometry occurring in quinonedimine moiety different from what can be expected from the biphenyl, while the similarity between the central part of the *O*DA molecule and quinonedimine is maintained, the group of N-C bonds remains planar. The earlier geometry results were obtained from crystallographic structure of complex with *O*DA. This geometry is consistent with the analysis of the frontier orbitals, confirming that the HOMO level of *O*DA and LUMO levels of heme are mainly localized over two nitrogen atoms of amino group of the central biphenyl core and C*HB* atom of the δ-meso heme edge. The difference in HOMO/LUMO gap energy between 5.7 eV for *O*DA and 4.9 eV for *O*DA quinonedimine is the same electronic configurations at different geometries. The lower value of 0.8 eV integrate the information given by the geometry, showing the substantial difference between the strain reduction processes taking place in *O*DA with respect to binitrogen of quinonedimine and obtained from the results of energy calculations on the basis of AM1 calculations.

The frontier orbital approach based on the structure of cyanide [R409L] complexes with *O*DA also suggests that it is enough to transfer electron from the HOMO ([-7.60eV; -7.72eV]) of *O*DA cation radical with the electrophilic Sr (0.372, 0.352) to the LUMO ([-1.62 eV; -1.42eV]) of the nucleophilic C*HB* in heme with nucleophile Sr (0.863, 1.017) greater than that of WT (0.832, 0.912). The HOMO/LUMO difference between *O*DA cation radical and C*HB* is of 5.98eV, respectively, and 6.3eV between A and B subunits as shown in Table 3. As suggested by the energy gaps, ET may complete and its cation radical can generate from neutral *O*DA.

The *O*DA acts as the cation radical (▪$^{+}$) and is poised for attack by the carbon atom (C*HB*) of δ-meso heme edge. The present work also gives evidence for an essential role of C*HB* as the KatG-typical active site on the *peroxidatic* activity. The LUMO energy of C*HB* has the nucleophilic reactivity with and plays a role in binding with *O*DA of which the HOMO has the electrophilic and forms a positive charge or lone electron pair on N atom in amino groups. Therefore, it is suggested that the *peroxidase* activity reflects advantageously on the binding affinity. Involvement of the HOMO of the (electrophilic) cationic amino group of *O*DA in the compound I is oxidized by the C*HB* of the (nucleophilic) anionic heme group, and an increase in the cavity volume through decay of π-complex between W95 and heme which cause a loss of the *catalase* reaction, may account for the increased *peroxidatic* activity and more catalytic efficiency of *kcat/Km* because of easier binding of *O*DA than that of WT. The redox intermediate compound I, which has iron oxidized to Fe^{4+}=O (oxyferryl species), is formed and a second oxidation equivalent as either a porphyrin cation radical (the LUMO energy of C*HB*) or the HOMO energy of *O*DA cation radical, which are phase-matched orbital in respective subunits.

On the other hand, the MO calculation based on structure of cyanide [R409L] is predictive that the unpaired electrons are localized on the iron (IV)-oxo moiety and on W95 by one electron shift of the unpaired electron from W95 to the porphyrin (C*1C*) near α–meso heme edge. In the absence of *O*DA, porphyrin cation radical (▪$^{+}$) (LUMO energy for C*1C* heme of -1.56eV; -1.42eV) has the nucleophilic Sr (0.636, 0.612) greater than that of WT (0.613, 0.583) with the initial formation of anion (-) heme group rather than W95 protein radical (HOMO for Nε1 W95 [-7.57eV and -7.54eV]) has formed the electrophilic Sr (0.275, 0.281) less than that of WT (0.285, 0.283). The respective energy gap between HOMO and LUMO has 6.01 eV and 6.13eV, ET can be complete occurring within 6eV (Pearson et al., 1986) of the energy gap for the excitation of the electron. The favourably stable neutral radical formation at W95 with concomitant loss of *catalase* function is followed by due to reduced stabilization of the iron (IV)-oxo containing compound II and increased reversion to compound I when ET in porphyrin ring has been implicated from C*1C* to C*HB*. It that a reduction in the cavity volume is suggested through occurrence of π-π* interaction between W95 and heme, which cause a loss of electron with concomitant of reversion to resting state during the *catalase* reaction, may account for reverting Compound II to Compound I with faster and slower rate of turnover of *O*DA, respectively, than that of WT in spite of increasing *peroxidatic* activity and more catalytic efficiency of *kcat/Km*. Since *O*DA cation radical (▪$^{+}$) is more erratic and unstable than W95 protein radical, if *O*DA is able to reach the active site (C*HB*), the *peroxidase* reaction occur in close proximity to the C*HB* after the ferry oxygen abstracts proton from *O*DA. We have identified a variant, R409L, which provides direct evidence for a bifurcated pathway in which *O*DA is

able to reach the active site (C*HB*) of heme, and is able to be oxidized by Compound I or Compound II heme intermediates. The presence of substrate is necessary to switch from *catalase* to *peroxidase* activities.

		Cyanide [R409L]			Cyanide [R409L]–*O*DA complex	
Subunit		A	B		A	B
	Electron source					
HOMO(eV)	M244(>S▪+)	-7.30	-7.54	M244	-7.78	-7.44
LUMO(eV)	G99Y101Y218	-2.62	-2.11	G99Y101Y218	-2.19	-2.04
HOMO-LUMO gap (eV)		4.68	5.43		5.6	5.4
phase	binding			binding		
Interaction	6th coordinate			Geometry of	Centred M244	
compound I reversion	but not *catalase*					
HOMO(eV)	W95Nε1(▪Trp)	-7.57	-7.54			
LUMO(eV)	(Por▪)C*1C*	-1.56	-1.42			
The H/L	Energy gap(eV)	6.01	6.12			
phase Interaction	anti-binding π-π*	3.4Å	3.4Å			
				Peroxidase		
HOMO(eV)			*O*DA(▪+)	cation radical	-7.60	-7.72
LUMO(eV)			C*HB*	nucleophilic	-1.62	-1.42
HOMO-LUMO gap(eV)					5.98	6.30
phase Interaction	binding π-π*				3.3Å	3.3Å

Table 3. Atomic orbital (a) HOMO and (b) LUMO Compositions of the MO for active site in R409L Cyanide Complexes with or without *O*DA. The geometries, phases and energies of the states would lead to *peroxidase* with the intramolecular interactions (coordinate, π–complexes, covalent and H–bonds) within van der Waals contacts and the limited energy gap.

3.4 MO study based on the structures of S305A complexes with or without SHA

Tripartite architecture is involved in the *catalase* function, which composed of the first π-complex between W95 residue and heme, the second covalent adduct of M244–Y218–W95 and the nearly octahedral coordinate complexes among G99, Y101 and M244. As first component stacks of alternating donor and acceptor residues are found in the *Hm*KatG. The relative orientations within the parallel planes of these residues are determined by the energies and charge distributions of the [HOMO] from which an electron will come, and the [LUMO] to which the electron will go. As presented in Table 4, both energies of [E (HOMO)] and [E (LUMO)] were calculated using the AM1 Hamiltonian, of which PM3, PM5 and PM6 wave functions (Stewart, 1989a; 1989b; 2007) denotes the same tendency. The [HOMO] energy represents the ionization potential of the indole ring in W95, i.e. the [E (HOMO)] of the negative value required to transmit an electron to [E (LUMO)] in heme edge of the porphyrin ring. (In such ET complexes the interplanar spacing of the flat residues is smaller than the normal spacing is of 3.4Å or can be equal to 3.1 Å). It is considered that ET has occurred in such donor-acceptor complexes. The indole ring of W95 in the covalent adduct is almost coplanar with the heme and the "general" ET is likely to occur to the lowest unoccupied heme orbital from the highest occupied π-orbital of W95. When LUMO/HOMO interactions are phase-matched energy gap with small difference between HOMO and LUMO, as well as strong intermolecular interactions, ET can be complete.

3.4.1 Third component (sulfur cation radical formation) in WT *Hm*KatG, [S305A] variants with and without SHA

Since the central S*δ* atom in side M244 of third component makes use of six d^2sp^3 hybrid orbitals, the shape is expected to be octahedral. Octahedral molecule geometries of sulfur coordination complexes have its steric number of 6. When five ligands can be used with a lone electron pair ":" in the octahedral system, an nearly octahedral arrangement complex around the S*δ* is created with the five ligands which contains two C atoms in the ethylmethylsulfide group of M244, two O atoms of G99 and Y101, and C*ε1* atom of the phenol side chain of Y218. The O atom of Y101 and C*ε1* atom of Y218 takes up an axial position of octahedral SO_2C_3":", whereas one O atom of G99, two C atom of ethylmethylsulfide group and a lone pair electron may take up the equatorial position. When the central S*δ* atom contains more than 6 electrons, the extra electrons form a lone electron pair. If a cation, charged 1+, gathers 6 equivalent ligands around it, S^+L_6, then each of these anions contributes a partial negative charge of -1/6 to the area around the cation, so that local electroneutrality results. For example, if each oxygen atom will experience 1/6 of the charge of the S^+ ion ($=1/6^+$) and S ion will experience 1/6 of an electron ($=0.16^-$) from each carbon and oxygen atoms, since a sulfur ion $S^+(0.96+)$ for WT is surrounded by two carbonyl oxygens and three carbon atoms in G99–C=O (0.47^-) and G101–C=O (0.51^-), Cε2(0.48^-) in Y218, Cγ(0.39^-), and Cε (0.45^-) which each of partial charge was calculated in M244 (SATO et al., 2011a; to be submitted). This value of 1/6 is called a bond valence of surrounding anions, respective atom was added a ground-state orbital slightly larger than the bond valence of 0.16^- or at least 0.2^-, which provides a value for the strength of each interaction between a cation and various anions. The shorter $S^+\cdots O$ interactions would be assumed to be stronger, with a greater partial charge donated by the oxygen atom to the S^+ ion in order to attain electroneutrality and to maintain the $S^+\cdots O$ distances that in S305A

(SATO et al., 2011c) are of [2.86 Å and 2.89 Å for C=O of G99] and [3.14 Å and 3.21Å for C=O of Y101] which about equal to [2.9Å and 2.85Å of G99] and [3.14Å and 3.28Å of Y101] in the subunit A, relatively, and B of WT. But the distances between S in M244 and C=O in G99 have longer M244_$S^+\cdots$O_G99 for SHA-S305A (2.91Å; 2.91Å) than that of S305A (2.86Å; 2.89Å) whereas shorter M244_$S^+\cdots$O_G101 for SHA-S305A (2.98Å; 3.08Å) than that of S305A (3.14Å; 3.21Å). When the SHA bound to [S305A], the electronegativity of O ligand atom of G99 in equatorial position of octahedral coordination was acquired by ET from S^+ with maintenance of electropositivity M244. At the same time, ET occurred to the M244 from the O atom of Y101 and C*ε1* atom of Y218 of an axial position. By close to Y101 and extension of Y218, electron from lone paired electron of S^+ was divided to W95 at one end of the covalent adducts, the W95 cation radical was caused by electron localization which electron transmitted to W95 from G99 and Y101 through Y218.

Electron must flow from the donor [HOMO] to the acceptor [LUMO], which need to be relatively close (~6eV) in energy (Pearson, 1986). As shown in Table 4, in [S305A] and SHA– [S305A], the sulfur center atom of M244 and the coordinate ligand atoms of carbonyl oxygen atoms of backbone G99 and Y101 plus phenol carbon of side Y218 have [E (HOMO) =-7.15, -7.41; -7.34, -7.88 eV] and [E(LUMO)=-2.52, -2.76; -2.91, -2.87eV], respectively. However, in spite of HOMO, sulfur atoms can be estimated as nucleophilic fr (0.192, 0.379; 0.336; 0.13), nucleophilic Sr (1.263, 1.004; 3.241, 1.141) as well as HOMO density (0.127, 0.217; 0.195, 0.085), and then may fill both roles as HOMO and LUMO by exhibiting the sulfur-ion complexation for MOPAC-specific calculation. In such a coordinate ligand as the carbonyl oxygen atoms of backbone G99 and Y101 plus phenol carbon atom of side Y218, there is also nucleophilic Sr in addition to only HOMO density and electrophilic fr. Thus the third component becomes an excellent source of electron, which an electron was transferred to attractive destination for W95 by way of the second component. Qualitatively, the properties and reactions of indoles have been explained by the resonance theory. π–electrons of an aromatic system is approximated as a linear combination of the functions of suitable contributing LUMO nucleophic phenol coordinate to HOMO electrophilic sulfur center structure and then may produce the electrophilic Sr and positive charge on nitrogen atom in indole group of side W95, reflecting the known electron-donating properties of the indole nitrogen.

3.4.2 First component (π–complex between W95 and heme formation) in S305T, S305A with or without SHA

At first component it was predicted from the MO calculation that a direct ET from W95 to heme and back donation took place during the *catalase* reaction as a result of a strong electronic interaction between W95 and heme. As shown in Table 2, the W95 π-orbital in [S305T] became both HOMO and LUMO while heme is just the contrary, exhibiting *catalase* activity. The W95 π-orbital became the HOMO of the complex system in cyanide [R409L] and [S305A], as shown in Tables 2, 3 and 4. The electron orbital is also best explained by the ET from the HOMO of W95 to the LUMO of C*1C* near α–meso heme edge. Although a transition between W95 orbital and C*1C* atomic orbital near the point of attachment was a strong contributor to the lower-energy level, when the accepting orbital on the δ–meso heme edge had no contribution from W95, including the LUMO of C*HB* as acceptor made a complete preparation for ET from *peroxidase* substrate, therefore no π-π* interaction has

favorably shifted from LUMO energy levels of C*1C* to C*HB*, allowing ET to the LUMO of C*HB* (from the HOMO of *O*DA as *peroxidase* substrate to be bound). The C*HB* is poised for nucleophilic attack by the amino nitrogen lone pair of *O*DA.

		WT	WT	S305A	S305A	SHA-S305A	SHA - S305A
	Subunit	A	B	A	B	A	B
LUMO(eV)	SHA					**-0.33**	**-0.51**
HOMO(eV)	Heme C*HB*					**-7.66**	**-7.69**
HOMO - LUMO gap (eV)						7.33	7.18
Phase						binding	binding
ET						impossible	impossible
LUMO(eV)	Heme C*HB*	-1.73	**-1.96**	**-1.83**	**-1.75**	**-1.98**	**-2.33**
LUMO(eV)	Heme C*1C*	**-1.59**	**-2.27**	**-1.34**	**-1.48**	**-1.52**	**-1.47**
HOMO(eV)	W95Nε1	**-7.92**	**-8.20**	**-7.55**	**-7.69**	**-7.8**	**-7.99**
The π-π* energy gap (eV)		6.33	5.93	6.21	6.21	6.33	6.52
Phase		bonding	bonding	bonding	bonding	bonding	bonding
ET		possible	possible	possible	possible	possible	possible
LUMO(eV)	G99 Y101 Y218	-2.86	-2.84	-2.52	-2.76	-2.91	-2.87
HOMO(eV)	M244	-7.32	-7.48	-7.15	-7.41	-7.34	-7.88
HOMO - LUMO gap (eV)		4.46	4.64	4.63	4.65	4.43	5.01
Phase		binding	binding	binding	binding	binding	binding
ET		Possible	possible	possible	possible	possible	Possible

Table 4. Computer-calculated parameters representative of the one-electron oxidation between porphyrin ring of Heme and either indole ring of W95 or aromatic inhibitor of SHA.

The calculated energies between HOMO of *O*DA and LUMO of C*HB* show that ET occurs in the [R409L] complex with *O*DA molecule. The transition from the ground to the first excited state and is mainly described by one-electron excitation from the HOMO of *O*DA (•+) cation radical to LUMO of C*HB*. The LUMO ":" of π nature, (i.e. porphyrin ring) is delocalized over the whole C–C bond. The HOMO is located over >C=N (•+) H atom of *O*DA quinonedimine, consequently the HOMO→LUMO transition implies an ET to aromatic part

of π-conjugated system from =NH group. Moreover, these orbitals significantly overlap. The HOMO–LUMO energy gap reveals that they are closely bound and both phase matched therefore become lower in energy. The net effect of ET from the HOMO to LUMO must correspond to the π-π* interaction bonds to be broken in the *peroxidase* reaction, instead of the π-bonds between W95 and heme to be made during the *catalase* reaction. In [S305A] variant structure, the potential ET is evident from the energies gap between orbital suggestive of [E (HOMO) =-7.55; -7.68 eV] on the indole nitrogen atom (N*ε1*) of W95 involved with nuclophilic Sr (0.331, 0.329) and [E (LUMO) =-1.34; -1.48 eV] on the carbon atom (C*1C*) electrophilic characteristics associated with nucleophilic superdelocalizability (0.676, 0.675) of the heme in the third component. In contrast, in the SHA-[S305A] complexes it was suggestive of an impossible ET from [E(HOMO)=-7.8; -7.99 eV] on the N*ε1* to [E(LUMO)=-1.47;-1.47eV] on the C*1C* due to deficiency in π–π* interaction formation of first component (Pearson RG. 1986). Despite the success of disrupting the π-complexes between heme and W95, one electron will require to be excited by more than 7eV of energy difference from [E (HOMO) =-7.66;-7.69 eV] on the (C*HB*) carbon of heme edge to [E (LUMO) =-0.33;-0.51 eV] on the SHA without electrophilic Sr, which is of *O*DA in *O*DA-[R409L]. It was guided by MO calculation that the LUMO of SHA and the HOMO of C*HB* of δ-heme edge cannot act as the electron donor, respectively, and the acceptor. It is indicative of MO results that SHA act as inhibitor, when HOMO/LUMO occurs in reverse from heme to SHA against the order from *O*DA to heme.

3.5 [R409L] structure based molecular orbital study with *O*DA and CN

It was predicted by [R409L] structure-based calculation that the new band originated as a result of a strong electronic interaction between *O*DA and *δ*-meso carbon (C*HB*) in δ–heme edge by 5.98–6.3 eV than that of N*ε1* of W95 and C*1C* near α–meso heme edge by 6.01–6.12 eV (Table 3). The former gap energy became more than the latter, increasing the *peroxidase* and reducing the *catalase* activities. If SHA serve as hypothetical substrate despite the original inhibitor, a direct ET from SHA to heme would not able to take place during the *peroxidase* reaction by 7.33–7.18eV (Table 4), since [S305A] cannot have the less gap energy than that of 6.21eV and then exhibits the *catalase* activity, which added a ground-state π-orbital slightly above the valence bond edge. A transition between SHA orbital and C*HB* with strong contributions from Fe (3d) atomic orbitals of heme near the point of attachment may also be too strong contributor to generate the new lower-energy band. SHA acts as inhibitor but not substrate, since it has not electrophile Sr which is essential for electorphilic characteristics of *O*DA to transfer an electron to nucleophilic *CHB* during *peroxidase* reaction process.

When the accepting orbital of C*1C* near the α– meso heme edge, including the LUMO, had no contribution from W95, it can be explained by allowing hole transfer from C*1C* to C*HB* in the δ–heme edge that the C*HB* π-orbital became the LUMO of the combined system and so ET was complete from *O*DA to C*HB* . But the reverse is hardly the case. The interaction has unfavorably changed HOMO and LUMO energy levels, not allowing ET to the LUMO of SHA from the HOMO of the C*HB*. The calculated HOMO of the C*HB* and LUMO of the SHA energies show so high that ET cannot occur in the molecule.

The *peroxidase* reaction has lower activation energy of the phase matched bonding orbital than that of *catalase* in [R409L]. A small HOMO-LUMO energy gap reveals a more reactive

compound of *peroxidase* substrate ligand than that of covalent adduct, which antibonding orbital has out –of –phase interaction and then are higher in energy than bonding orbitals that combine to produce binding interactions. A compound of substrate ligand as *O*DA with a small HUMO-LUMO energy gap could be considered as a soft base, since the electrophilc Sr of ODA (0.372, 0.352) has also the greater than that of Nε1 in W95 (0.275, 0.281) whereas the C*HB* (0.863, 1.017) exhibits much greater nucleophilic Sr than that of C*1C* (0.636, 0.612).

This three-part structural feature may generally occur in KatG molecules, over quite long distances from M244 via W95 to C*HB* at the heme edge, where an electron is localized by disrupting the π-conjugated system between N*ε1* of W95 and C*1C* near the heme edge. Then C*HB* become the LUMO orbital to accept an electron from *peroxidase* substrate. The energy gap of C*HB* in the transition- iron-based heme is determined by the π-π* energy difference from property inherent in *peroxidase* substrate, but cannot be tuned regardless of π-π* splitting between W95 and heme. Therefore, the inhibitor ligand as SHA attached to the transition iron is relatively small. The π-conjugated system of SHA can be made smaller by including ferryl oxygen [Fe^{4+}=O] within the conjugated system of heme than that of as *O*DA. The ferryl oxygen lowers the excited-state energy owing to a stronger electron affinity relative to carbon. Small π-chromophores such as SHA are used to inhibit resting (π-ground) and compound II (π*-excited) states of heme *peroxidase*. It involves a direct transition from the π-ground state into the heme, by passing the π*-excited state, which is high in energy.

In the *catalase* reaction, it would be, for instance, an electron in the HOMO of W95 is transferred to the LUMO of the heme by way of the "hot spot" between heme (C*1C*) and W95(N*ε1*). In the *peroxidase* reaction, the HOMO→LUMO transition implies an ET from the HOMO of *O*DA as a donor molecule to the LUMO of the heme (C*HB*) as acceptor. An ET prone part of heme and ODA is common in site, where has the large gap and is of opposite phase in LUMO orbital to SHA as inhibitor and the *O*DA*red* as product. The pathway is suggested by suppression of ET from the HOMO of C*HB* to the LUMO of SHA and the ODA_{red}, of course, as the contradiction is untrue. The hydroxamic acid oxygen atom (-NH-OH) of the SHA is thought to be of [-0.33 for subunit A and -0.51 eV for B] as LUMO electron acceptor but in fact acts as HOMO nucleophilic Sr (0.345, 0.358) rather than LUMO electrophilic Sr (0.286, 0.240). The C*HB* in the δ-meso carbon and ferryl oxygen por (•+) cation radical is of [-7.66 – -7.69eV] which is considered to be electron donor as HOMO nucleophilic Sr (0.860, 0.766). It should give the intermolecular space to the possible ET mechanism of *peroxidase* reaction that distance between the -NH-OH oxygen atoms of SHA and the nitrogen atom of cyanide heme Fe is shorter than those the ferryl oxygen atom of Fe^{IV}=O of CCP(Itakura et al.,1997) .

The distance between the hydroxamic acid oxygen atom of aromatic donor and the oxygen atom of Fe^{IV}=O is 1.5–1.6Å in KatG, 3.3Å of BHA and 3.4Å of SHA in ARP. These distances are shorter than those of cytochrome C system or CCP (Poulos et al., 1993). Therefore SHA cause to inhibit the KatG.

3.6 [M244A] structure based docking and frontier orbital studies with H_2O_2, SHA and *O*DA

Both k_{cat} (the rate of turnover) and K_m values (affinity) for H_2O_2 to [M244A] cannot be detected from kinetic study (Ten-i et al., 2007; SATO et al., 2011d). From the docking study,

however, H_2O_2 binding affinity can be estimated and the proposal space (§3.1 *vide supra* in Fig.3 (A)) among three target residues can be predicted as W95, H96 and D125 from the docking energies which each subunit A and B is of (-30.3kcal/mol; -23.9kcal/mol) for W95, (-29.9 kcal/mol; -18.2 kcal/mol) for H96 and (-32.1 kcal/mol;-30.3kcal/mol) for D125. It is suggested by the structure-based calculation that [M244A] variant has almost the same as affinity for H_2O_2 between subunit A and B, respectively.

A calculated binding energy of subunit A for -76.5 kcal/mol also reveals to have significantly 2-fold higher affinity for inhibitor SHA than that of B for -30.9 kcal/mol. In subunit A, SHA acts as an inhibitor of compound II with respect to a substrate aromatic donor. It is conceivable that SHA behaves as a substrate of compound II but does not imply the competitive binding with other donor such as *O*DA due to binding at the different sites in reactions with compound II intermediate. In the subunit B, SHA bind to the resting state when an ionisable carbonyl group of D125 with pKa value of 4 is not protonated. It is deduced that SHA also inhibits compound I formation by retarding H_2O_2 binding the iron. A possible inhibitor binding site has been proposed for target residue D125, in a cavity on the distal side of the δ- meso heme edge as shown in Fig.5.

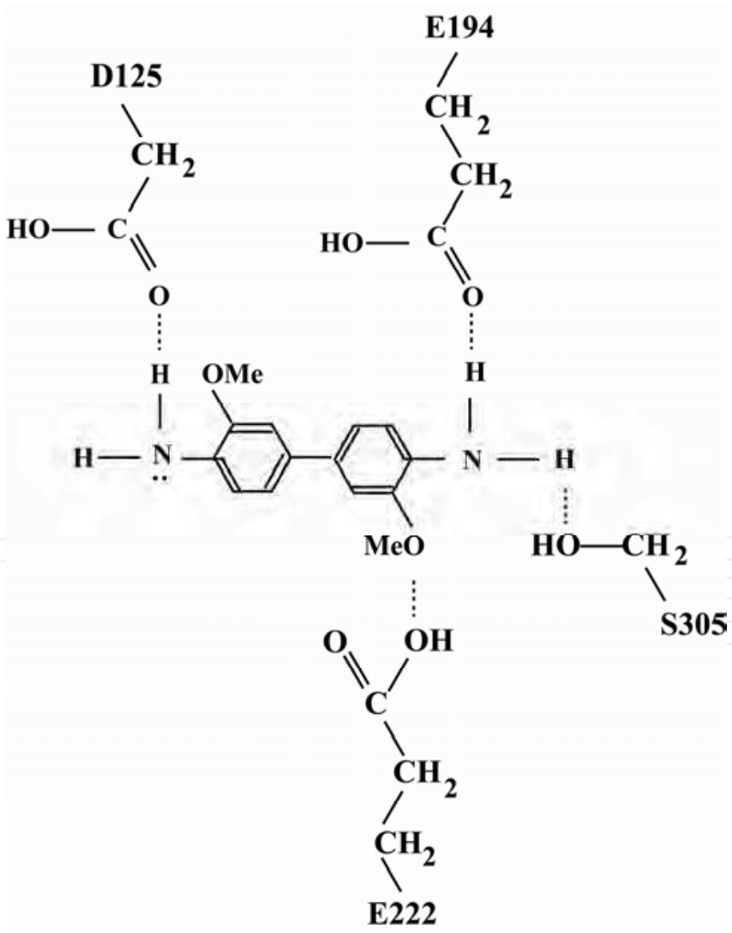

Fig. 4. The Bind Site Predicted from Docking Calculation with *O*DA and Confirmed X-ray Structure of Complex.

As shown in Fig.4, the proxy end N atom of the amino side chain in substrate *O*DA is H-bonded with the Oδ*2* atom of D125 in the heme distal pocket. The opposite end N atom forms salt bridge with the side-chain of E194, the carboxyl group of E222 and the carbonyl oxygen atom of backbone S305, with the flexible side chain and without distortion of main chain after binding *O*DA. The *O*DA affinity would be increased by the displacement of the side chain of D125 and E194, two active residues on LL1 loop. Oxidation of *O*DA at nitrogen atom of quinoneimine groups can be also shown by reaction 6 as illustrated in scheme 1.

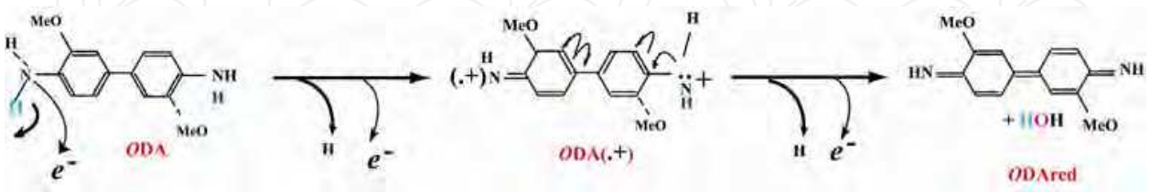

Scheme 1.

Indeed the specific enhancements in *peroxidise* isoenzyme pattern can be influenced by the *O*DA affinity difference between each subunit. The binding site of another *peroxidise* substrate as *O*DA cation radical (*O*DA (·$^+$) had been estimated with -46.6 kcal/mol from docking calculations against D125 for subunit A but expected from repulsive energy for subunit B in Table 5. Thus it can be postulated that the active site of subunit A exhibits the higher affinity for the imino (>C=NH) group of *O*DA (·$^+$) and deprotonate the amino (-NH_2) group of *O*DA more efficiently than that of the subunit B. The difference of catalytic efficiency in M244A here is of the 18 fold higher subunit A than that of B (Sato et al., 2011d). It has established that subunit B may be correlated with the slow rate of Compound I formation and the fast rate of reduction of Compound II. Subunit A occur the reduction of compound II and can release the product molecule as ODA_{red} resulting from complete reaction of the *peroxidase*, if subunit A of compound II may adsorb *O*DA (·$^+$). Subunit B cannot has the *catalase* reactivity but regenerate compound I, since its compound II is insensitive to H_2O_2 and desorbed *O*DA (·$^+$).

M244A						
Subunit	A	B	A	B	A	B
	initiator		inhibitor		substrate	
Ligand	H_2O_2		SHA		*O*DA	
Target residue						
W95 (kcal/mol)	-30.3	-23.9				
H96 (kcal/mol)	-29.9	-18.2				
D125 (kcal/mol)	-32.1	-30.3	-76.5	-30.9	-46. 6	repulsive
Heme (kcal/mol)	-26.6	-23.9	-69.3	-26.9		

Table 5. Binding Energies for *Hm*KatG [M244A] Variant Associated with Initiator H_2O_2, Inhibitor SHA and *Peroxidise* Substrate *O*DA.

As shown in Table 6, it is supported by the frontier orbital calculation for M244A that *catalase* activity lost when ET cannot complete between C*1C* carbon and N*ε1* nitrogen atom. Though the C*1C* carbon atoms [for subunit A of -0.96eV and B of -1.27eV] of the heme is of LUMO orbital balanced with existing nucleophilic Sr (0.523,0.771), the C*1C* can shrink neither less than 3.3 Å nor always link the *π-π* interaction to W95, if W95 N*ε1* (·+) cation radical show transient HOMO orbital on the covalent adduct of Y218–W95 [-7.57eV, respectively, and -7.62eV] with electrophilic Sr (0.462, 0.518), since both energy gaps exceed the capacity of ET over 6 eV. C*HB* carbon atoms of heme are of LUMO in subunit A [-1.87eV] and B [-1.39V] and also exhibit nucleophilic Sr (1.113, 0.924). It is possible to recognize as the *peroxidase* substrate with the presence of the *O*DA. However, without the *O*DA in especially subunit B of M244A, Compound I and W95 were elaborated by ET to W95 (•+) cation radical with electrophilc Sr from Por(•+) via π-complex between them. It is suggested that the C*1C* coexist with HOMO density, electrophilc fr and electrophilic Sr. When electron donation to the W95(•+) cation radical is made from (•-)C*1C* atom on Por (•+), compound II reverts to compound I. The working hypothesis of the present study therefore includes the assumption that outcomes of the structure-based calculations can be used as a role to assist reproduction of compound I in *peroxidase* reaction.

			M244A			
	Subunit		A		B	
HOMO(radical)	Y218- W95	Nε1(·+)	-7.57eV		-7.62eV	
LUMO+1	Heme	C*1C*	-0.96eV		-1.27eV	
The energy gap & distance			6.61eV	3.9Å	6.35eV	3.3Å
Phase & ET			bonding	impossible	bonding	possible
LUMO(nucleophilic)	Heme	C*HB*		-1.87eV		-1.39V

Table 6. Each Subunit of MO Energy in the π-complexes with Y218-W95 covalent adduct of *Hm*KatG [M244A] Variant

Geometry, which used for the calculations of its model compounds I and II ,was consist of 15 residues which included in R92, W95, H96, G99, T100, Y101, D125, N126, I217, Y218, A244, H259, S305, R409, and heme. In subunit B, the orbital between C*1C* Heme and N*ε1* W95 become the binding orbital (in green and yellow) and promotes the bonding of π-system of indole rings of Trp and pyrole ring of heme, which may be reclaiming compound I. In subunit A, the two atoms between N*ε1* W95 and C*1C* Heme is distantly-positioned from 3.9Å, which opposes the π-bonding interaction and cannot transfer electrons, even if each orbital (in red and blue) are attractive and may normally overlap between the bonding molecular orbital. Therefore the reduction of compound II would occur when *O*DA (·+) cation radical bound to C*HB*.

Despite a lack of *peroxidase* substrate in [M244A] variant, no *catalase* reactivity against the second H_2O_2 exhibits at all so that the electron cannot transfer from M244 to the covalent adducts W95 via Y218. In spite of a π-π* electron interaction of the heme with W95 in the covalent adduct, the ability to transfer electron between an electrophile of tyrosinate of

Y218 and the nucleophile of sulfur cation was lost by the deletion mutation at the position 244. Therefore KatG is considered the *catalase* function to use a methionine nucleophile intramolecularly- and octahedrally-coordinated complexes with the carbonyl O atoms of Y101 and G99 as well as known to use tyrosinate–indole electrophiles (Carpena et al., 2005). Crystallographic analysis of *Hm*KatG [M244A] variant as indicated that the Y218 could move its side chain closer to the indole group of W95 in subunit B (SATO et al., 2011d). It was suggested that oxygenation of heme (compound I) was activated in ET where heme formed π-complexes with W95 in the covalent adduct, and reduction of ferryl-intermediate by *O*DA was activated in resting (ferric) KatG. This suggestion is supported by MO calculations for [M244A] that compounds I and II would be sufficient to initiate substrate oxidation as *O*DA. As summarized in the scheme shown in scheme 2, a proposed mechanism for twice the one-electron oxidation of *O*DA substrate to the radical product (*O*DA·$^{+}$) by KatG intermediate is presented as follows: one electron could transfer from compound II (*A2*) reduction back to the resting state (*C1*) and another electron could be attribute to converse compound I (Fe^{IV}=O) (*B1*) to the compound II (Fe^{IV}-OH) formation (*A1*) in Subunit A. It is common to both subunit A and B. While exhibiting the isoenzyme pattern of *peroxidase* reaction, it is indicated as the bifurcated pathway that this recoverable form of compound I (*B2*) occurs directly from the activated form of compound II (*A1*) in Subunit B. It has proposed for KatG that M244A mutation effectively follows the *peroxidase* dual pathway.

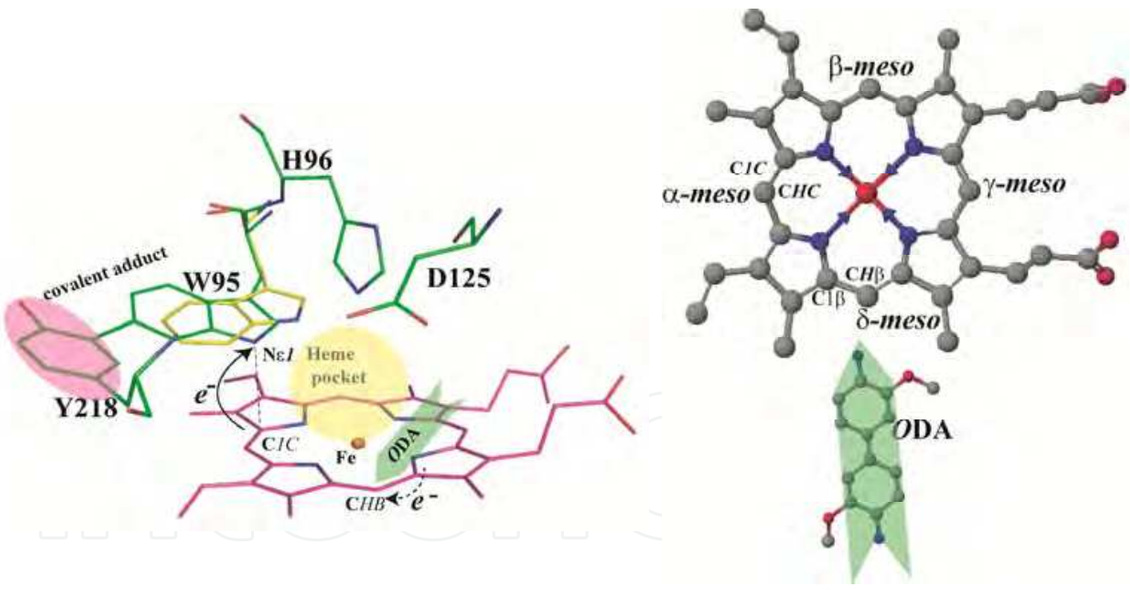

(a) (b)

Fig. 5. Electron Transfer in iron Protoporphyrin IX (heme) and the Adduct or *O*DA. View showing the stacking of the indole ring of W95 on 3.25Å above pyrol ring C of heme (left panel). The intramolecular ET from porphyrin to the covalent adduct can be explained by the formation π-complexes with W95 ($^{\bullet+}$) and heme, having reverted to compound I from the compound II with no substrate. If *O*DA is bound to C*HB* of δ-heme edge, it allows electron from *O*DA to the heme to promote oxidation by substrate *O*DA. Structure of heme and *O*DA (right panel). This nomenclature is consistent with using in crystallographic work. The figures were constructed using Pymol (DeLano, 2002).

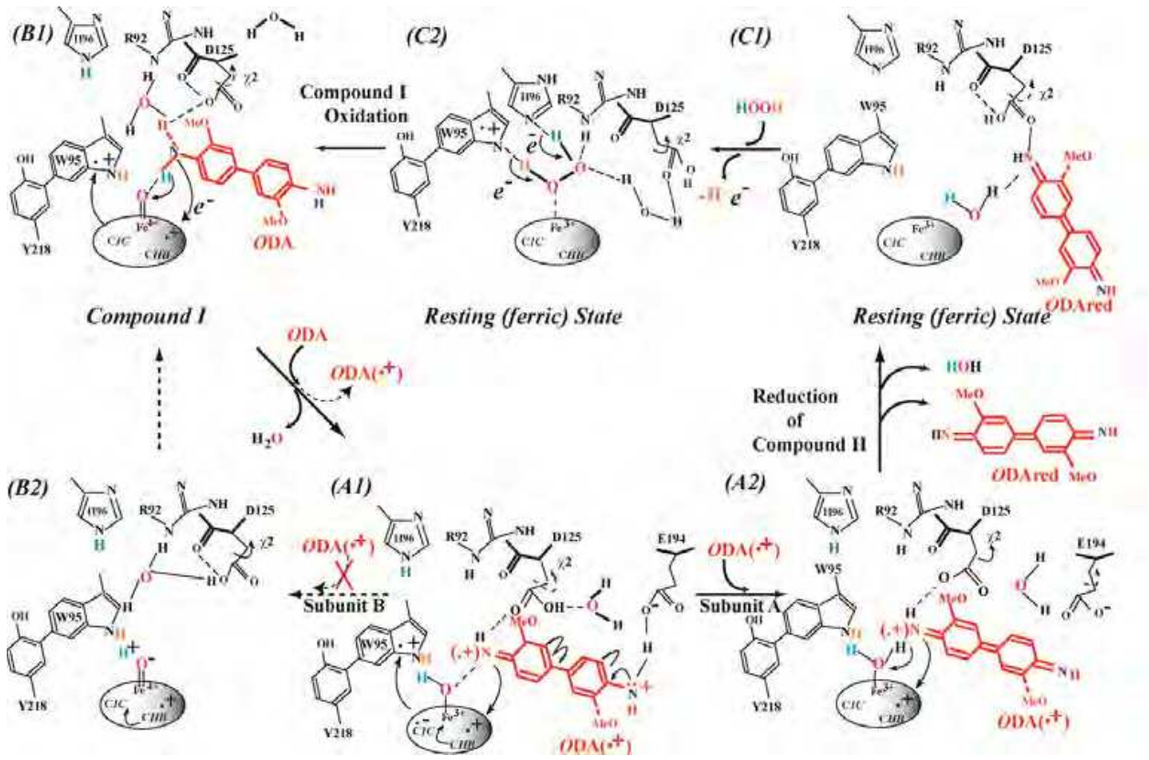

Scheme2. Summary of the Effect of the [M244A] Mutation on the Scheme Combined Compound I Regeneration of Subunit B and the Reduction of Compound II of Subunit A. Showing the involvement of key active site residues of [M244A] variant, compound II can decay into one of two active forms. The Compound II in the active center of subunit B can be converted back to compound I (*B2*) without rebinding the inverted *O*DA(·+) cation radical, proceeding to the left, but the *peroxidase* reaction, proceeding to the right from Compound II (*A1*) in the active center of subunit A with binding inverted *O*DA(·+) results in conversion to resting state (*C1*). The initiator H_2O_2 molecule involved in the Compound I oxidation (*B1*), and the substrate *O*DA (·+) involved in the reduction of compound II (*A2*) are shown in potential H-bonded conformations.

4. Conclusion

Crystal structure of *Hm*KatG has been first determined by 2.0Å resolution and reported the proposal structural characteristics of covalent adduct between Sδ of M244–Cε2 of Y218 and Cε1 of Y218–Cη2 of W95 in maintaining the *catalase* activity of the KatG (Yamada et al., 2002). The residues which make up the active site catalytic triad are highly conserved in all KatGs, identified both through functional studies and by comparison with homologues identified in sequenced genomes. X-ray analysis of other KatGs, including *Mt*, indicates that the corresponding residues are also arranged in a similar catalytic triad. Crystal structure analysis has demonstrated that the Met variant significantly affects W95 in the protein structure on the distal side of the heme since slight changes were observed for the puckering (shrinking and stretching of the interatomic bonds between) heme C*1C* –N*ε1* of indole ring as compared to the WT protein (Heering et al., 2002; Santoni et al., 2004).

However, unlike these Met variants from other sources, in the *Hm*KatG [M244A] variant the *catalase* activity was not detected at all but *peroxidase* activity was even enhanced. All the reported kinetic constants (rate of turnover, k_{cat}, the affinity of substrate, K_m, and catalytic efficiency, k_{cat}/K_m) of otherwise KatG for *catalase* and *peroxidase* activities are "apparent" values as conventional *Catalase* and *Peroxidase* do not follow typical Michaelis-Mentan kinetics. Kinetic parameters for *catalase* and *peroxidase* are determined by fitting the kinetic data to non-linear (mixed) Michaelis-Menten equation and show that isoenzyme pattern of active two catalytic center motifs typical of *catalase* and *peroxidase*. That's the reason why KatG is a functional heterodimer in governing KatG dimeric subunits structure.

Crystal structure of the [M244A] variant of *Hm*KatG was of not identical subunits (SATO et al., 2011d). Subunit A disrupted a possible π-interaction between W95 and heme. Including the differences in active site geometry, it would be sufficiently stronger to facilitate the oxoferryl (Fe (IV) =O) reduction in the *peroxidase* reaction. And back donation of electron from heme edge to W95 would suffice for compound I revitalization in subunit B, suggesting from HOMO/LUMO energy gap and nucleophilic Sr of Nε*1* based on S305T structure (SATO et al., 2011a).

Characterization of the electron path may identify each site of electrophilic W95 Nε*1* and nucleophilic heme C*1C* in *Hm*KatG and influence of heme C*HB* on *peroxidase* substrate reduction. Further functional studied with the use of X-ray crystal structure based calculation has given to better understanding of ET pathways and radical formation sites in KatG. This approach was investigated how frontier molecular orbital theory applies to either the inhibitory of a SHA (SATO et al., 2011c; to be submitted) or the reactivity of *O*DA compounds (SATO et al., 2011b; to be submitted) with, respectively, single and double phenolic ring. For SHA binding, the side-chain of D125 is rotated around the dihedral angle χ1 by 100.8° whereas *O*DA binding affinity was enhanced by χ2 of 61.3°of D125 residue. On the contrary, in subunit B, the consequent ET from heme to W95 could explain the enhancement of *peroxidase* and iteratively-generated compound I intermediate. The isoenzyme pattern of *peroxidase* was discussed in terms of its hetero-dimeric character of *peroxidatic* subunit A for reduction of compound II and subunit B for reclaiming compound I. The value of catalytic efficiency (k_{cat}/K_m) for the *peroxidatic* reaction catalyzed by the *Hm*KatG [M244A] variant falls within the expected range for an efficient enzyme (Albery & Knowles, 1976).

The M244–Y218–W95 covalent adduct confirms to be essential for the *catalase* activity in *Hm*KatG as well as *Mt*KatG (Ghiladi et al., 2005b; 2005c). It was also constructed to explore the effect of successive triple-base substitutes for Met244 to Ala and to cleavage the covalent bond amongst the tripeptide. The [M244A] variant that coupled with the structure based-evolution within laboratory time scale is not biochemically associated with INH susceptibility. Despite of INH resistance-conferring variants, this “unnatural” protein engineering for *Hm*KatG, can confirm the inherent *catalase* functional capability of the *C-ter* end of *E- helix* in KatG. Perhaps the most intriguing feature of the *Mt*KatG is its ability to mediate INH susceptibility. In our current working hypothesis for the cause of isoenzyme pattern of *peroxidase* activity, it is suggest that the drug interacts with the enzyme and is converted by the *peroxidase* activity into a toxic derivative which acts at a second, as yet unknown, site (Zhang,Y., et al., 1992).

Clearly, further experiments are required to address this hypothesis. For a better understanding of the complex interrelations between *catalase* and *peroxidise,* the oxidation of phenols, in the present paper some studies on the kinetic characterization of this enzyme in bacterials has been carried out with the detection of KatG isoenzyme patterns. Whereas *C-ter* capping by positively charged M244 residues in *E-helix* is effective to neutralize the helix dipole which lead to destabilization of the helix through entropic effect. Since it may be less effective to neutralize the *B-helix* dipole, the electron can transfer to carbonyl oxygen atoms of *C-ter* capping with G99 and Y101 residues in *B-helix* from heme via the W95–Y218 covalent linkage adduct with M244 centred octahedral coordinate. Just as *O*DA analogous compounds are bound D125, E194 and E222 on mobile LL1 loop, as the destabilization or cleavage of the covalent adduct linkage between M244 and Y218 may be caused by the mobile Y218 which located on the upstream residues of LL1 loop in binding site. Since the competitive inhibition of *O*DA substrate may imply in binding SHA inhibitor (as hypothetical INH), the right candidates of the INH may be narrowed down and selected out in a great number of these lead compounds, if the higher binding and lower activation energies for ET during *peroxidase* reaction are predicted by further docking and additional *ab initio* MO calculations based on the structure of binding site of INH-sensitive (*peroxidase*) KatG variants. *Peroxidases* are highly polymorphic enzymes, and the functionality of each isoenzyme depends on its (acidic) nature and its persistent growth phase of the *Mt* clinical strains. In order to facilitate the *peroxidase* activity and to understand the metabolic functions that are needed for the persistence of *Mt*, compounds that could eradicate persisters effectively can be useful in the design of HIV/anti-tuberculosis drugs.

5. Acknowledgements

The author wish to thank Mr. W. Higuchi for excellent technical assistance, Dr. K. Yoshimatsu for preparing *Hm*KatG variants and Prof. T. Fujiwara for providing recombinant KatG from *Haroarcula marismortui* from the Department of Biological Sciences at Shizuoka University. I thank also Gorana Screrbe for her expert secretarial assistant and for helpful discussions during the preparation of this manuscript.

6. References

Albery, E.J., and Knowles, J.R. (1976) Evolution of enzyme function and the development of catalytic efficiency. *Biochemistry* Vol.15, pp. 5631-5640, ISSN 0006-2960

Bertrand, T., Eady, N.A.J., Jones, J.N., Jesmin, J.M., Nagy, J.M., Jamart-Gregoire, B., Raven, E.L., Brown,K.A. (2004) Crystal structure of Mycobacterium tuberculosis *catalase-peroxidase*. The *Journal of Biological Chemistry* Vol.279, pp.38991-38999, ISSN 0021-9258

Carpena, X., Wiseman, B., Deermagarn, T., Singh, R., Switala, J., Ivancich, A., Fita, I., and Loewen,P.C. (2005) A molecular switch and electronic circuit modulate *catalase* activity in *catalase-peroxidase*s *EMBO Report* Vol.6, pp.1156-1162, ISSN 1469-221X

DeLano, W. L. (2002) The PyMOL Molecular Graphics System, DeLano Scientific, Palo Alto, CA

Dewar M.J.S., Zoebisch E.G., Healy E.F., and Stewart, J.J.P. (1985) Development and use of quantum mechanical molecular models. 76. AM1: a new general purpose quantum

mechanical molecular model. *Journal of the American Chemical Society* Vol.107, pp.3902-3909, ISSN 0002-7863.

Dobner P., Rüsch-Gerdes S., Bretzel G., Feldmann K., Rifai M.,Löscher T., and Rinder H. (1997) Usefulness of *Mycobacterium tuberculosis* genomic mutations in the genes katG and inhA for the prediction of isoniazid resistance. Int J Tuberc Lung Dis Vol.1, pp365-369, ISSN 1027-3719

Fukui, K., Yonezawa, T., and Nagata, C. (1954) Theory of Substitution in Conjugated Molecules. *Bulletin of the Chemical Society of Japan*, Vol.27, pp.423-427, ISSN 0009-2673

Fukui, K., Yonezawa, T., and Nagata, C.(1957) MO-Theoretical Approach to the Mechanism of Charge Transfer in the Process of Aromatic Substitutions. *The Journal of chemical physics*, Vol.27, pp.1247-1259, ISSN 0021-9606

Fukuzawa, K., Kitaura, K., Nakata, K., Kaminuma, T., and Nakano, T. (2003) Fragment molecular orbital study of the binding energy of ligands to the estrogen receptor. *Pure and Applied chemistry*, Vol.75, pp.2405-2410, ISSN 1365-3075

Ghiladi, R.A., Cabelli, P.R., and Ortiz de Montellano,P.R. (2004) Superoxide reactivity of KatG: Insights into isoniazid resistance pathways in TB. *Journal of the American Chemical Society* Vol.126, pp.4772-4773, ISSN 0002-7863

Ghiladi, R.A., Medzihradszky,K.F., Rusnak,F.M., and Ortiz de Montellano,P.R. (2005a) Correlation between isoniazid resistance and superoxide reactivity in Mycobacterium tuberculosis KatG. *Journal of the American Chemical Society* Vol.127, pp.13428-13442, ISSN 0002-7863

Ghiladi, R. A., Knudsen, G. M., Medzihradszky, K.F., and Ortiz de Montellano, P. R. (2005b) The Met-Tyr-Trp Cross-link in *Mycobacterium tuberculosis Catalase-peroxidase* (KatG). *The Journal of Biological Chemistry* Vol. 280, pp. 22651–22663, ISSN 0021-9258

Ghiladi, R. A., Medzihradszky, K. F., and Ortiz de Montellano, P. R. (2005c) Role of the Met-Tyr-Trp Cross-Link in *Mycobacterium tuberculosis Catalase-Peroxidase* (KatG) As Revealed by KatG(M255I). *Biochemistry*, Vol.44, pp.15093-15105, ISSN 0006-2960

Heering, H. A., Indiani, C., Regelsberger, G., Jakopitsch, C., Obinger, C., and Smulevich, G. (2002) New Insights into the Heme Cavity Structure of *Catalase-Peroxidase*: A Spectroscopic Approach to the Recombinant *Synechocystis* Enzyme and Selected Distal Cavity Mutants., *Biochemistry* Vol.41, pp. 9237–9247, ISSN 0006-2960.

Haas W.H., Schilke K., Brand J., Amthor B., Weyer K., Fourie P.B., Bretzel G., Sticht- Groh V., and Bremer H.J. (1997) Molecular analysis of katG gene mutations in strains of *Mycobacterium tuberculosis* complex from Africa. *Antimicrob Agents Chemother* Vol.41, pp.1601-1603, ISSN 0066-4804

Heym, B., Zhang, Y., Poulet, S., Young, D., and Cole, S. (1993) Characterisation of the KatG gene encoding *catalase-peroxidase* required for the isoniazid susceptibility of Mycobacterium tuberculosis. *Journal of Bacteriology.*, Vol.175, pp.4255-4259, ISSN 0021-9193

Heym B., Alzari P.M., Honoré N., and Cole S.T. (1995) Missense mutations in the *catalase-peroxidase*, katG are associated with isoniazid resistance in *Mycobacterium tuberculosis. Molecular microbiology* Vol.15, pp.235-245, ISSN 0950-382X

Hillar, A., Peters, B., Pauls, R., Loboda, A., Zhang, H., Mauk, A.G., and Loewen, P.C. (2000) Modulation of the Activities of *Catalase−Peroxidase* HPI of *Escherichia coli* by Site-Directed Mutagenesis. *Biochemistry* Vol.39, pp.5868-5875, ISSN 0006-2960

Ikeda-Saito M., Shelly D.A., Lu L., Booth K.S., Caughey W.S. and Kimura S. (1991) Salicylhydroxamic acid inhibits myeloperoxidase. *J.Biol.Chem.* Vol.266, pp.3611-3616, ISSN 0021-9258

Itakura H., Oda Y., Fukuyama K. (1997) Binding mode of benzhydroxamic acid to arthromyces ramosus *peroxidase* shown by X-ray crystallographic analysis of the complex at 1.6 Å resolution. *FEBS Letters* Vol.412, pp.107-110, ISSN 0014-5793

Ivancich, A., Jakopitsch, C., Auer, M., Un, S., and Obinger, C. (2003) Protein-Based Radicals in the *Catalase-Peroxidase* of *Synechocystis* PCC6803: A Multifrequency EPR Investigation of Wild-Type and Variants on the Environment of the Heme Active Site. *Journal of the American Chemical Society* Vol. 125, pp. 14093–14102, ISSN 0002-7863

Jakopitsch, C., Auer, M., Regelsberger, G., Jantschko, W., Furtmüller, P.G., Ruker, F., and Obinger, J. (2003a) Distal site Aspartate is Essential in the *Catalase* Activity of *catalase-peroxidase*s. *Biochemistry* Vol.42, pp.5292-5300, ISSN 0006-2960

Jakopitsch, C., Auer, M., Ivancich, A., Ruker, F., Furtmüller, P.G., and Obinger, J. (2003b) Total conversion of bifunctional *catalase-peroxidase* (KatG) to Monofunctional *peroxidase* by exchange of a conserved distal side tyrosine. *Journal of Biological Chemistry* Vol.278, pp.20185-20191, ISSN 0021-9258

Jakopitsch, C., Ivancich, A., Schmuckenschlager, A., Wanasinghe, A., Furtmüller, P.G., Ruker, F., and Obinger, C. (2004) Influence of the unusual covalent adduct on the kinetics and formation of radical intermediates in Synechocystis *catalase peroxidase*: A stopped-flow and EPR chracterization of the Met275, Tyr249, and Arg439 variants. *Journal of Biological Chemistry* Vol.279, pp.46082-46095, ISSN 0021-9258

Marttila H J., Soini H., Eerola E., Vyshnevskaya E., Vyshnevskiy B. I., Otten T. F., Vasilyef A. V., and Viljanen M. K. (1998) A Ser315Thr substitution in KatG is predominant in genetically heterogeneous multidrug-resistant *Mycobacterium tuberculosis* isolates originating from the St Petersburg area in Russia. Antimicrob Agents Chemother Vol.42, pp.2443-2445, ISSN 0066-4804

Modi S., Behere D.V., and Mitra S. (1989) Binding of aromatic donor molecules to lactoperoxidase: proton NMR and optical difference spectroscopic studies. *Biochim.Biophys.Acta* - Proteins and Proteomics Vol.996, pp.214-225, ISSN 1570-9639.

Musser J.M., Kapur V., Williams D. L., Kreiswirth B. N., van Soolingen D., van Embden J.D.A. (1996) Characterization of the *catalase-peroxidase* gene (katG) and inhA locus in isoniazid-resistant and susceptible strains of *Mycobacterium tuberculosis* by automated DNA sequencing: restricted array of mutations associated with drug resistance. *The Journal of Infectious Diseases* Vol.173, pp.196-202, ISSN 0022-1899.

Pearson R.G. (1986) Absolute electronegativity and hardness correlated with molecular orbital theory. *Proceedings of the National Academy of Sciences of the United States of America* Vol.83, pp.8440-8441, ISSN 0027-8424

Petersen M.R. and Csizmadia I.G. (1979) Determination and analysis of the formic acid conformation hypersurface. *J.Amer.Chem.Soc.* Vol.101, pp. 1076-1079, ISSN 0002-7863

Poulos, T.L., Edwards,S.L., Wariishi,H., and Gold,M.H. (1993) Crystallographic refinement of lignin *peroxidase* at 2Å. *Journal of Biological Chemistry*, Vol. 268, pp.4429-4440, ISSN 0021-9258

Regelsberger, G., Jakopitsch, C., Rüker, F., Krois, D., Peschek, G. A., and Obinger, C. (2000) Effect of Distal Cavity Mutations on the Formation of Compound I in Catalase-Peroxidases. *Journal of Biological Chemistry*, Vol. 275, pp.22854-22861, ISSN 0021-9258

Saint-joanis, B., Souchon, H., Wilming, M., Johnsson, K., Alzari, P.M., and Cole, S.T.(1999). Use of site-directed mutagenesis to probe the structure, function and isoniazid activation of the *catalase/peroxidase*, KatG, from *Mycobacterium tuberculosis. Biochemical Journal* Vol.338, pp.753-760, ISSN0264-6021.

Santoni, E., Jakopitsch, C., Obinger, C., and Smulevich, G. (2004) Manipulating the covalent link between distal side tryptophan, tyrosine, and methionine in *catalase-peroxidase*s: An electronic absorption and resonance Raman study. *Biopolymers* Vol.74, pp. 46–50, ISSN 1097-0282.

Sato, T., Higuchi, W., Yoshimatsu K., and Fujiwara, T. *Catalase* Functional Implication Guided by Structure, Docking, Molecular Orbital and Kinetics Studies on Ser305Thr and Arg409Leu variants of *Hm*KatG (2011a; to be submitted)

Sato, T., Higuchi, W., Yoshimatsu K., and Fujiwara, T. Crystal Structures and *Peroxidatic* Function of Cyanide Arg409Leu (R409L) Variant and its Complexes with *o*-Dianisidine (*O*DA) in KatG from *Haloarcula Marismortui*. (2011b; to be submitted)

Sato, T., Higuchi, W., Yoshimatsu K., and Fujiwara, T. Crystal Structure and Kinetics Studies on Ser305Ala variant of KatG from *Haloarcula Marismortui* and its Complexes with Inhibitor SHA (2011c; to be submitted)

Sato, T., Ten-i, T., Higuchi, W., Yoshimatsu K., and Fujiwara, T. Crystal Structure and Kinetic Studies on Met244Ala [M244A] Variants of KatG from *Haloarcula Marismortui*. (2011d; to be submitted)

Singh, R., Wiseman,B., Deemagarn,T. Donald,L.J., Duckworth,H.W., Carpena,X., Fita,I., and Loewen,P.C. (2004) *Catalase-peroxidase* (KatG) exhibit NADH oxidase Activity. *Journal of Biological Chemistry* Vol.279, pp.43098-43106, ISSN 0021-9258

Slayden, R.A. and Barry III, C.E. (2000) The genetics and biochemistry of isoniazid resistance in *Mycobacterium tuberculosis. Microbes and Infection* Vol.2, pp.659-669, ISSN 1286-4579.

Stewart J.J.P., (1989a) Optimization of parameters for semiempirical methods. I. Method, *Journal Computational Chemistry*, Vol.10, pp209-220, ISSN 1096-987X.

Stewart J.J.P., (1989b) Optimization of parameters for semiempirical methods. II. Applications, *Journal Computational Chemistry*, Vol.10 , pp221-264, ISSN 1096-987X.

Stewart J.J.P., Mopac 2002 release 2.1 Fujitsu Limited,Tokyo, JAPAN(2002)

Stewart J.J.P., (2007) Optimization of parameters for semiempirical methods V: Modification of NDDO approximations and application to 70 elements. *Journal of Molecular Modeling* Vol.13, pp.1173-1213,ISSN 1610-2940)

Ten-i, T., Kumasaka, T., Higuchi, W., Tanaka, S., Yoshimatsu, K., Fujiwara, T. and Sato, T. (2007) Expression, purification, crystallization and preliminary X-ray analysis of Met244Ala variant of *catalase-peroxidase* (KatG) from the haloarchaeon Haloarcula marismortui. Acta Crystallographica Section F Vol. 63, pp.940-943, ISSN 1744-3091

Wei, C.J., Lei,B., Musser, J.M., and Tu, S.C. (2003) Isoniazid activation defects in recombinant Mycobactrium tuberculosis *Catalase-Peroxidase* (KatG) mutants evident in InhA inhibitor production. *Antimicrobial Agents and Chemotherapy*, Vol.47, pp.670-675, ISSN 0066-4804

Wengenack N. L., Uhl J. R., St. Amand A. L., Tomlinson A. J., Benson L. M., Naylor S., Kline B. C., Cockerill III F. R., and Rusnak F. (1997) Recombinant *Mycobacterium tuberculosis* KatG (S315T) is a competent *catalse-peroxidase* with reduced activity toward isoniazid. *J Infect Dis* Vol.176, pp.722-727, ISSN 0022-1899

Welinder, K.G. (1991) Bacterial *catalase-peroxidase*s are gene duplicated members of the plant *peroxidase* superfamily. *Biochimica et Biophysica Acta - Proteins and Proteomics*Vol.1080, pp.215-220, ISSN 1570-9639.

Welinder, K.G. (1992) Superfamily of plant, fungal and bacterial *peroxidase*s. *Current Opinion in Structural Biology* Vol.2, pp.388-393, ISSN 0959-440X

Yamade,Y., Fujiwara,T., Sato,T., Igarashi,N., and Tanaka,N. (2002) The 2.0Å crystal structure of *catalase-peroxidase* from *Haroarcula marismortui*. *Nature Structural Biology* Vol.9, pp691-695, ISSN10728368

Zhang, Y., Heym,B., Allen,B., Young,D., and Cole,S. (1992) The *catalase-peroxidase* gene and isoniazid resistance of Mycobacterium tuberculosis. *Nature* Vol.358, pp.591-593, ISSN 0028-0836

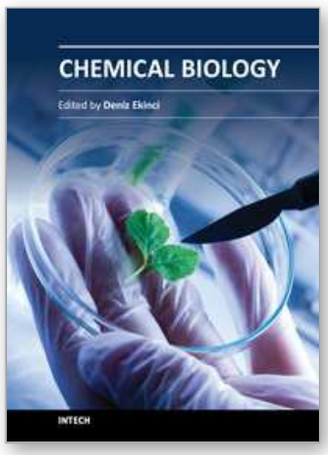

Chemical Biology

Edited by Prof. Deniz Ekinci

ISBN 978-953-51-0049-2
Hard cover, 444 pages
Publisher InTech
Published online 17, February, 2012
Published in print edition February, 2012

Chemical biology utilizes chemical principles to modulate systems to either investigate the underlying biology or create new function. Over recent years, chemical biology has received particular attention of many scientists in the life sciences from botany to medicine. This book contains an overview focusing on the research area of protein purification, enzymology, vitamins, antioxidants, biotransformation, gene delivery, signaling, regulation and organization. Particular emphasis is devoted to both theoretical and experimental aspects. The textbook is written by international scientists with expertise in synthetic chemistry, protein biochemistry, enzymology, molecular biology, drug discovery and genetics many of which are active chemical, biochemical and biomedical research. The textbook is expected to enhance the knowledge of scientists in the complexities of chemical and biological approaches and stimulate both professionals and students to dedicate part of their future research in understanding relevant mechanisms and applications of chemical biology.

InTech Europe
University Campus STeP Ri
Slavka Krautzeka 83/A
51000 Rijeka, Croatia
Phone: +385 (51) 770 447
Fax: +385 (51) 686 166
www.intechopen.com

InTech China
Unit 405, Office Block, Hotel Equatorial Shanghai
No.65, Yan An Road (West), Shanghai, 200040, China
中国上海市延安西路65号上海国际贵都大饭店办公楼405单元
Phone: +86-21-62489820
Fax: +86-21-62489821

IntechOpen